A01-34350

AIAA 2001-3665
Numerical Analyses on Pressure Wave Propagation in Repetitive Pulse Laser Propulsion

Hiroshi Katsurayama, Kimiya Komurasaki,
and Yoshihiro Arakawa
University of Tokyo, Tokyo, Japan

37th AIAA/ASME/SAE/ASEE
Joint Propulsion Conference & Exhibit
8-11 July 2001
Salt Lake City, Utah

AIAA-2001-3665

NUMERICAL ANALYSES ON PRESSURE WAVE PROPAGATION IN REPETITIVE PULSE LASER PROPULSION

Hiroshi KATSURAYAMA,* Kimiya KOMURASAKI† and Yoshihiro ARAKAWA‡
University of Tokyo, Hongo 7-3-1, Bunkyo, Tokyo 113-8656, Japan

Abstract

Pressure wave propagation in a repetitive pulse air-breathing laser thruster flying at Mach 5 flow has been computed in order to clarify the behavior of a shock wave induced by focusing laser beams in supersonic flow, as well as to estimate the impulse acting on the thruster. As a result, the detailed process of shock reflection on the body and the mechanism for thrust generation have been analyzed. Moreover, the estimated coupling coefficient, which is the cumulative impulse per one pulse of laser energy, has been found to be fairly constant at a value of approximately 150 N · s/MJ, being independent of the laser energy. Results also reveal that the coupling coefficient is sensitive to the focus location.

NOMENCLATURE

$C.A.R.$	=	capture area ratio
C_d	=	drag coefficient
C_m	=	coupling coefficient
D	=	aerodynamic drag
M	=	Mach number
S	=	area relative to body
e	=	total energy per unit volume or electron charge
h	=	flight altitude of vehicle
n_c	=	critical electron number density for cut-off
m_e	=	electron mass
p	=	static pressure
ρ	=	density
q	=	heat flux
R	=	air gas constant = 287J/kg
T	=	static temperature
t	=	time
u, v	=	axial, radial velocity component
z, r, θ	=	cylindrical coordinates
γ	=	specific heat ratio = 1.4
ϵ_0	=	dielectric constant of vacuum
η_{laser}	=	fraction of laser energy absorbed by plasma
τ	=	viscous stress tensor
ω_L	=	laser radiation frequency

subscripts

B	=	body part of vehicle
inC	=	inner cowl part of vehicle
inlet	=	inlet of vehicle
outC	=	outer cowl part of vehicle
∞	=	freestream property

*Graduate student, Department of Aeronautics and Astronautics, Student Member AIAA
†Associate Professor, Department of Advanced Energy, Member AIAA
‡Professor, Department of Aeronautics and Astronautics, Member AIAA

INTRODUCTION

Laser propulsion will serve as an alternative propulsion system for ground-to-orbit launch systems in the near future. Since energy is transmitted from the ground or from laser base in space to the vehicle and propellant is not needed during the air-breathing mode, the payload ratio becomes high. Therefore, the launching cost should be low. In addition, laser propulsion is free from fuel mixing and combustion problems in high speed flows.

Myrabo et al. proposed an axisymmetric laser thruster, so-called "Lightcraft," and conducted flight tests with a scaled model .[1,2] Two Lightcraft configurations exist: closed-inlet type and air-breathing type. The air-breathing type Lightcraft, with a weight of 50 g, has flown up to 30 m vertically and up to 121 m horizontally by using a repetitive pulse laser of 10 J per pulse and 10 Hz.

Wang et al. computed the flow in the Laser Lightcraft featuring a closed inlet.[3] Their computations included detailed physical models to clarify the laser-plasma interactions and the propagation processes of Laser Supported Detonation wave (LSD) and Combustion wave (LSC) in quiescent atmospheric air. These LSD and LSC mechanisms were investigated in detail by Raizer.[4–6] However, when the electron density reaches the critical value for cut-off, it is not clear what percentage of laser energy is absorbed by the plasma. Wang et al. assumed 40 % absorption and obtained a value for the impulse which agreed very well with the one measured by Myrabo et al..

In the present computation, the pressure wave propagation in the air-breathing laser thruster flying at Mach 5 is investigated. The shape of the thruster is almost identical to the one of the Laser Lightcraft.

It is assumed that the laser energy absorbed by the plasma is simply deposited at the focus. A detailed laser-plasma interaction model is not included in our present computation. Still, the pres-

sure wave propagation process is expected to be precisely reproduced at the given energy absorption.

LASER LIGHTCRAFT

The Laser Lightcraft consists of a nosecone forebody, a parabolic afterbody, and a cowl, as shown in Fig.1. The parabolic afterbody works both as an aerospike nozzle and as a focusing mirror. When a high-power pulsed laser beam is focused by the afterbody mirror, air-breakdown occurs at the ring focus on the cowl. Then, the annular shaped plasma produced near the focus absorbs the following part of the laser pulse and then grows. The expansion of this annular plasma generates a shock wave. The shock wave strikes the afterbody and the cowl, and expands through the aerospike nozzle. The former effect exerts the direct impulse on the afterbody and the cowl, and the latter effect becomes the additional impulse caused by expansion of the pressure wave through the nozzle. As the enthalpy of the plasma is converted into thrust through these processes, the repetitively transmitted laser pulses are converted into repetitive thrust impulses.

COMPUTATIONAL METHOD AND GRID

Governing equations

Although the temperature becomes very high after air-breakdown, air is assumed as a calorically perfect gas in all computations.

The Navier-Stokes equations are solved in axisymmetric cylindrical coordinates. The equations are expressed via an unsteady vector equation in conservative form.

$$\frac{\partial \mathbf{U}}{\partial t}+\frac{\partial \mathbf{F}}{\partial z}+\frac{\partial \mathbf{G}}{\partial r}=\frac{\partial \mathbf{M}}{\partial z}+\frac{\partial \mathbf{N}}{\partial r}+\mathbf{S}. \quad (1)$$

$$\mathbf{U}=\begin{bmatrix}\rho\\ \rho u\\ \rho v\\ e\end{bmatrix},\mathbf{F}=\begin{bmatrix}\rho u\\ \rho u^2+p\\ \rho uv\\ (e+p)\,u\end{bmatrix},\mathbf{G}=\begin{bmatrix}\rho v\\ \rho uv\\ \rho v^2+p\\ (e+p)\,v\end{bmatrix},$$

$$\mathbf{M}=\begin{bmatrix}0\\ \tau_{zz}\\ \tau_{zr}\\ u\tau_{zz}+v\tau_{zr}-q_z\end{bmatrix},\ \mathbf{N}=\begin{bmatrix}0\\ \tau_{zr}\\ \tau_{rr}\\ u\tau_{zr}+v\tau_{rr}-q_r\end{bmatrix},$$

$$\mathbf{S}=\frac{1}{r}\begin{bmatrix}-\rho v\\ -\rho uv+\tau_{zr}\\ -\rho v^2+\tau_{rr}-\tau_{\theta\theta}\\ -(e+p)\,v-q_r+u\tau_{zr}+v\tau_{rr}\end{bmatrix}. \quad (2)$$

The total energy per unit volume is defined as

$$e=\frac{p}{\gamma-1}+\frac{\rho\left(u^2+v^2\right)}{2}. \quad (3)$$

The equation of state for ideal gas being employed is,

$$p=\rho RT. \quad (4)$$

For the viscosity and thermal conductivity, the Sutherland formulas[7] for air are used. The values obtained by these formulas deviate from the actual values over 1900 K due to the effect of chemical reactions. To this respect, although the viscosity is about twice as large as Sutherland formula under the condition of 10,000 K and 1 atm,[8] this deviation is ignored in the present computations.

Numerical scheme

A cell-centered finite volume scheme is adopted. The inviscid flux is estimated with a AUSM-DV scheme[9] and extended to 3rd-order space accuracy is achieved employing a MUSCL approach[10] with Van Albada's flux limiter. The viscous flux is estimated with a standard 4th-order central difference. Time integration is performed with a LU-SGS scheme.[11] In order to avoid the complication of the boundary condition around the cowl, the flow field has been divided into four zones (Fig.1). Four points at the interface of each zone are overlapped. At the interface, 3rd order space accuracy is maintained by using the so-called Fortified Solution Algorithm.[12]

Computational grid

Figure 2 shows the computational grids. The configuration is almost the same as the one of the Lightcraft[1] proposed by Myrabo. The body length and its maximum radius are set to 20 cm and 6.75 cm respectively. The cowl is placed at 1.25 cm above the body shoulder and covers the body from $z = 10$ cm to $z = 16$ cm. The parabolic afterbody surface is designed to focus a laser beam on the inner cowl surface, at $z = 14$ cm, $r = 8$ cm. The grids are concentrated ahead of the forebody to clearly capture the bow shock, and between the cowl and afterbody so as to capture the propagation of the pressure wave after air-breakdown.

Boundary conditions

The freestream inflow condition is given as listed in table 1.

Table.1 Flight condition.

h	20km
M_∞	5
ρ_∞	8.89×10^{-2}kg/m^3
T_∞	216.65K

At the inflow boundary, all physical properties are fixed according to the supersonic inflow condition. In addition, the inflow is assumed to be parallel to the z axis.

At the body and cowl surfaces, slip and adiabatic wall conditions are adopted. Static pressure is determined by considering the curvature of the wall surface.

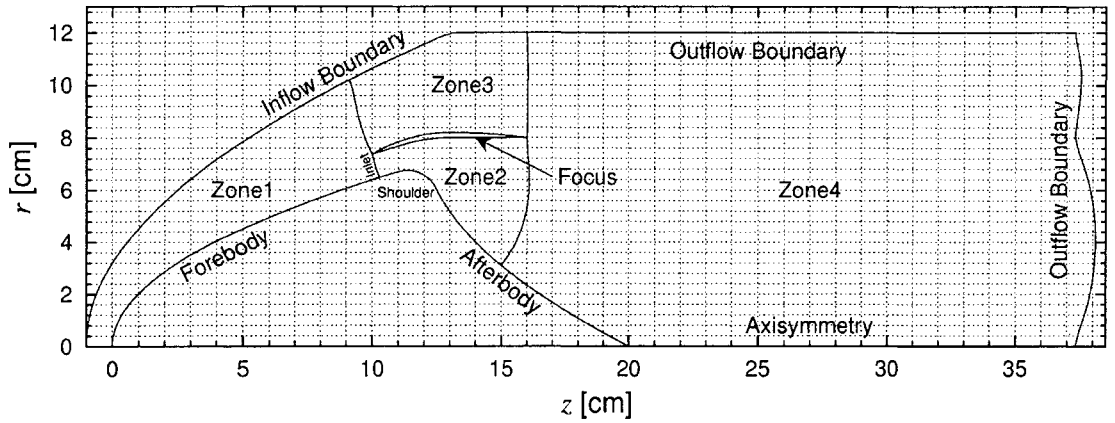

Fig.1 Lightcraft configuration and divided computational zones.

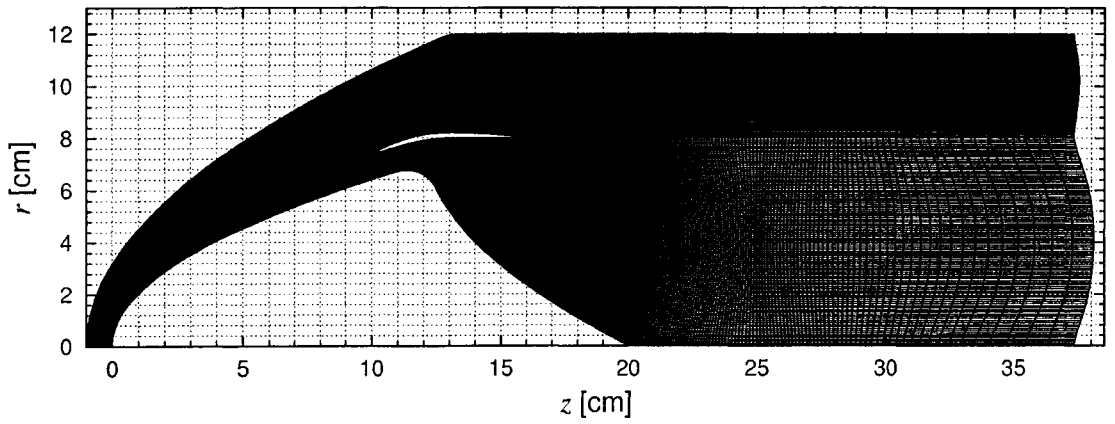

Fig.2 Computational grids.

Explosion source

When air-breakdown occurs at the focus, free electrons absorb the laser radiation by the Inverse Bremsstrahlung process and a high temperature plasma is produced. The expansion of this plasma induces a strong shock wave. The layer behind the shock front is ionized by shock heating, resulting in laser absorption in the shock layer. In this process, the strong shock wave propagates to the laser incident direction maintaining its intensity. This wave is referred to as LSD.[4] As the shock wave moves upstream toward the laser incident direction, the laser energy density decreases. When the laser energy density decreases to a critical value, the shock separates from the plasma front. The plasma front expands with subsonic speed because the electron heat conduction and radiation heat transfer enables the neighboring cold layer to absorb the laser radiation. This mechanism is referred to as LSC.[5]

However, in order to clarify the behavior of LSD and LSC, many physical models must be included in the numerical code. Still, to avoid a high computational cost, laser absorption processes are neglected in the present computation. The energy is assumed to be deposited on one numerical cell located at the ring focus, which is shown in Fig.1

When the electron density of the plasma front reaches the following critical value,

$$n_c = \frac{\epsilon_0 m_e \omega_L}{e^2}, \tag{5}$$

the laser beam cannot penetrate the plasma front. Then, the laser radiation is partially reflected or scattered off, and partially absorbed at the plasma front.[3] Unfortunately, this mechanism has not been clarified yet, and it can be said that it is very difficult to determine the portion of laser energy that is absorbed by the plasma. In the computations of Wang et al.[3], it is assumed that $\eta_{\text{laser}} = 40\%$ during this critical plasma resonance. The impulse estimated by their computation agreed very well with the experiments by Myrabo et al..

In the present computation, it is assumed that the plasma absorbs half the energy of one pulse laser energy,

$$\eta_{\text{laser}} = 50\%. \tag{6}$$

The laser energy absorbed by the plasma is simply deposited on the focus. Although this approach cannot assess the validity of η_{laser}, the pressure wave propagation process is expected to be precisely reproduced at the given energy absorption.

RESULTS AND DISCUSSION

Inital flow field

At first, steady state flow before laser-focusing is obtained. Figure 3 shows the pressure contours. The Capture Area Ratio[13] calculated by the following equation is a considerably low value, 31.3%.

$$C.A.R. = \frac{\iint_{S_{\text{inlet}}} \rho \boldsymbol{v} \cdot \boldsymbol{ds}}{\iint_{S_\infty} \rho \boldsymbol{v} \cdot \boldsymbol{ds}} \ . \qquad (7)$$

The S_{inlet} is the area between the cowl leading edge and the body shoulder. The S_∞ is the circle area calculated by taking the radius of the cowl leading edge. With respect to $C.A.R.$, this Lightcraft configuration may be more suitable to higher Mach number flow than $M_\infty = 5$.

After the flow passes through the bow shock, the Mach number is reduced to 2.5 at the inlet. Figure 4 shows the pressure contours and velocity vectors near the inlet. An oblique shock wave is generated at the cowl leading edge. After passing through this shock wave, the flow above the cowl is accelerated by a series of expansion waves which originate from the outer cowl surface. Between the cowl and the body, a series of compression waves originates from the inner cowl surface. On the body shoulder, the flow separates from the body surface. A shock wave originates at this separation point.

Figure 5 shows the pressure contours and velocity vectors from the vicinity of the cowl end to $z = 35$ cm. The wake caused by this separation spreads till $z = 27$ cm on the z axis. The velocity direction in the wake is opposite to the main flow direction.

The axial aerodynamic drag can be decomposed into the body part, D_{B}, the inner cowl part, D_{inC}, and the outer cowl part, D_{outC}. The D_{B}, D_{inC} and D_{outC} are 605 N, -88 N, 141 N, respectively and the total drag is 655 N. Although D_{inC} works as the positive force, the effect is small because most of the surface is parallel to the axial direction. The drag coefficient, C_d, is 0.37 if the representative area is taken as the area which is calculated by projecting the body and the cowl into the axial direction.

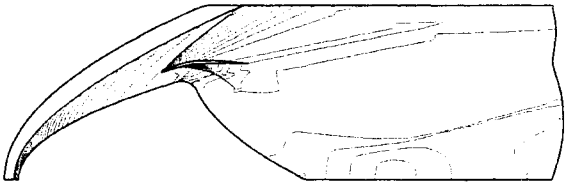

Fig.3 Pressure contours in the steady state flow field.
(max. = 180818 Pa, min. = 408 Pa, incre. = 3608 Pa)

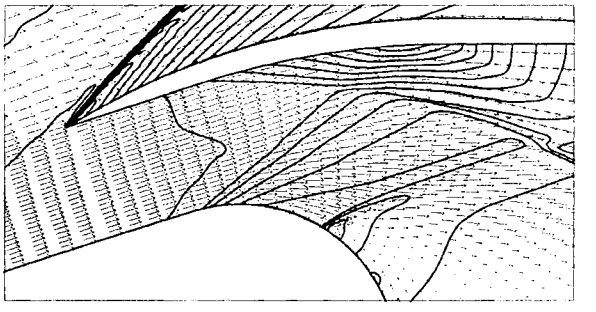

Fig.4 Pressure contours and velocity vectors near the inlet.

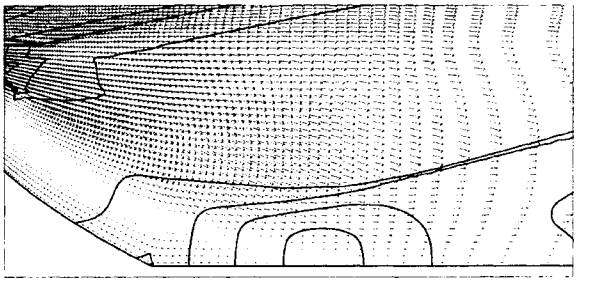

Fig.5 Pressure contours and velocity vectors from the vicinity of the cowl end to $z = 35$ cm.

Laser induced shock propagation

Three cases of laser-focusing with 200, 400 and 600 J energy are computed. The focus is located on the cowl surface. Since $\eta_{\text{laser}} = 50\%$ is assumed, the net deposited energy is half the value of laser energy. Figures 6(a) $\sim$ (f) show the pressure contours and velocity vector plots at $t = 0.5 \sim 15.0\mu$s with 400 J laser energy.

At $t = 0.5\mu$s, just after the laser-focusing, the induced shock wave is reflected on the cowl surface, and the shape of shock wave becomes features a half-torus shape. The distributions of physical properties in this region encompassed by the shock wave still resemble the self-similar solution of a point source.[14]

At $t = 2.5\mu$s, each of the legs of the shock wave begins to propagate with different speed; One of

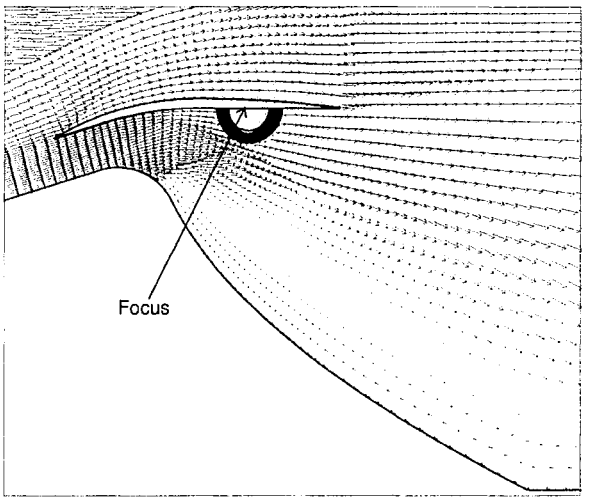

(a) t = 0.5 μs
(max. = 3743926 Pa, min. = 403 Pa, incre. = 74870 Pa)

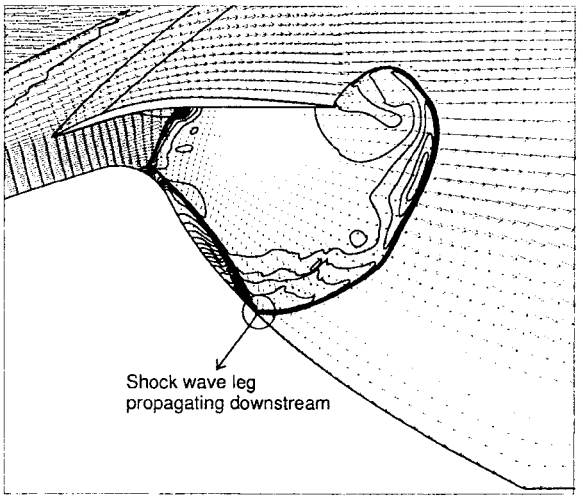

(d) t = 7.5 μs
(max. = 1488152 Pa, min. = 1153 Pa, incre. = 29740 Pa)

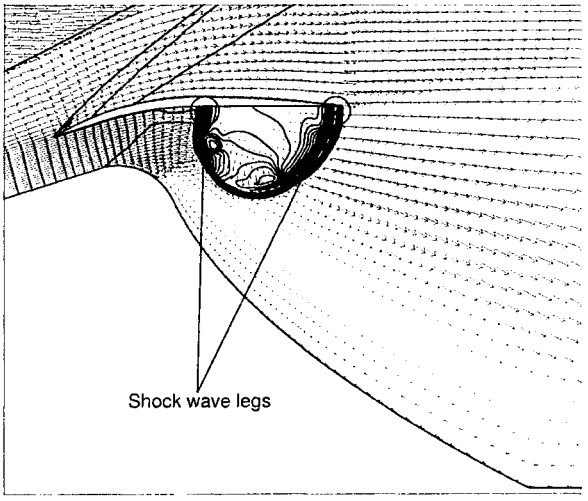

(b) t = 2.5 μs
(max. = 934008 Pa, min. = 405 Pa, incre. = 18672 Pa)

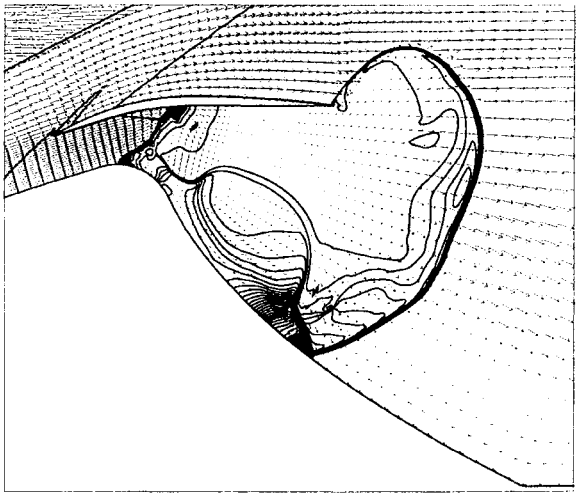

(e) t = 10.0 μs
(max. = 1207828 Pa, min. = 1399 Pa, incre. = 24129 Pa)

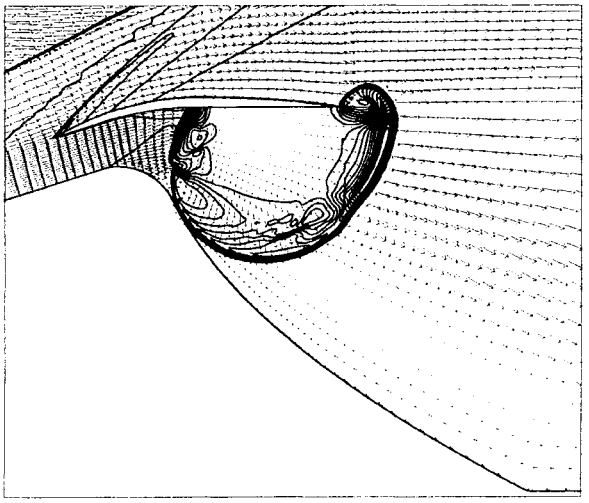

(c) t = 5.0 μs
(max. = 696236 Pa, min. = 411 Pa, incre. = 13917 Pa)

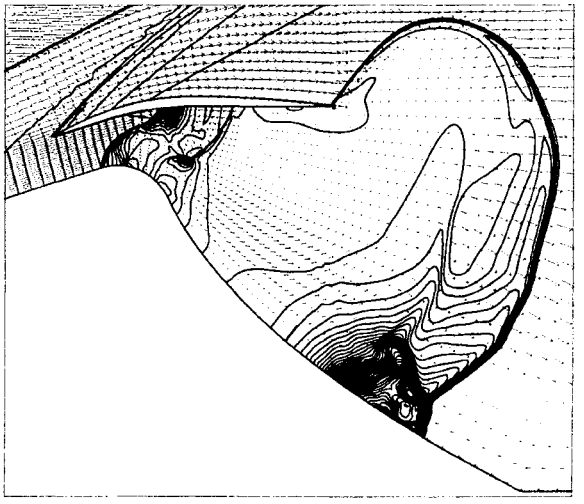

(f) t = 15.0 μs
(max. = 647684 Pa, min. = 1400 Pa, incre. = 12926 Pa)

Fig.6 Pressure contours and velocity vectors at $t = 0.5 \sim 15.0$ μs in the case of laser-focusing on the cowl with 400 J energy.

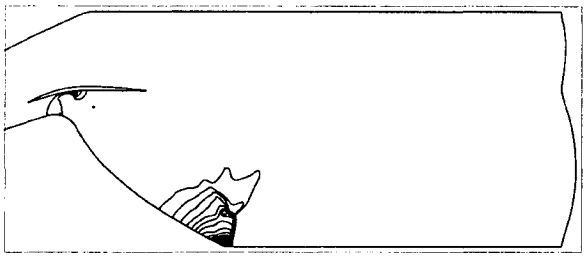

(a) t = 20 μs
(max. = 3550556 Pa, min. = 1400 Pa, incre. = 70983 Pa)

(e) t = 60 μs
(max. = 103193 Pa, min. = 157 Pa, incre. = 3613 Pa)

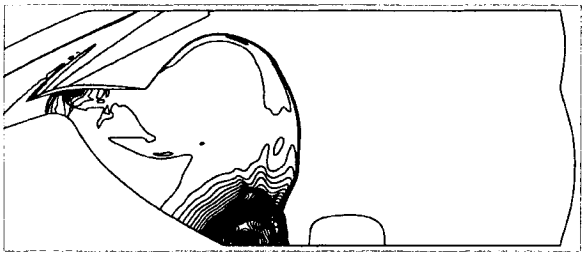

(b) t = 25 μs
(max. = 637040 Pa, min. = 1400 Pa, incre. = 12712 Pa)

(f) t = 70 μs
(max. = 86716 Pa, min. = 3 Pa, incre. = 3616 Pa)

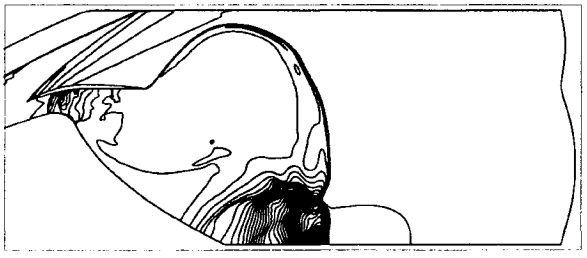

(b) t = 30 μs
(max. = 540184 Pa, min. = 1421 Pa, incre. = 10775 Pa)

(g) t = 100 μs
(max. = 46978 Pa, min. = 200 Pa, incre. = 3612 Pa)

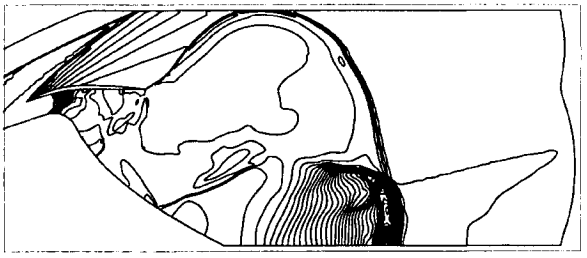

(c) t = 40 μs
(max. = 321745 Pa, min. = 1736 Pa, incre. = 6400 Pa)

(h) t = 300 μs
(max. = 46978 Pa, min. = 47 Pa, incre. = 3615 Pa)

(d) t = 50 μs
(max. = 134052 Pa, min. = 1962 Pa, incre. = 3577 Pa)

Fig.7 Pressure contours at $t = 20 \sim 300$ μs in the case of laser-focusing on the cowl with 400 J energy.

them moves upstream against the inflow, and the other moves downstream with higher speed since it rides on the flow.

At $t = 5.0\mu$s, the shock wave strikes the afterbody and the entire inflow is compressed by the shock.

At $t = 7.5\mu$s, the shock wave leg propagating downstream appears on the afterbody. At $t = 7.5 \sim 15\mu$s, this shock wave leg sweeps the afterbody and the pressurized region on the afterbody becomes wide. By these processes, the Lightcraft obtains the main thrust. During this sweep, a regular reflection of shock appears on the afterbody and the pressure at the reflection point reaches maximum at each instant. The regular reflection transits to Mach reflection as reported in many experiments and computations.[15] On the other hand, the shock wave propagating upstream stays near the inlet because the shock wave propagation speed relative to the body becomes equal to the inflow speed. Due to a similar reason, the shock wave near the cowl end also stays there.

Figures 7(a) $\sim$ (h) show the pressure contours at $t = 20 \sim 300\mu$s. At $t = 20\mu$s, the shock wave leg reaches the afterbody tail. Although the pressure at this point rapidly increases because of the axisymmetrical shock focusing, the thrust level does not increase so much. The reason is that the inclination of the afterbody tail to the axial direction is small and the pressurized region by this shock-focusing is narrow. This peak of pressure stays near the afterbody tail for a while, shown in 7(b). After times larger than $t = 25\mu$s, the height of the triple point gradually increases and the Mach stem propagates downstream.

On the other hand, the shock wave near the inlet gradually begins to be blown downstream and decays to the pressure waves.

The small Mach stem observed at $t = 50\mu$s would be generated by the re-concentration of pressure waves blown from the inlet. The shock wave attaching at the cowl end separates at $t = 70\mu$s and then is blown downstream. At $t = 100 \sim 300\mu$s, the flow field almost returns to the steady state.

Influence of focus location

To examine the influence of the focus location on the flow field, the laser beam is assumed to be focused at the point ($z = 0.14$ cm, $r = 6$ cm) which is located in the middle of the flow channel, regardless of the afterbody shape.

With 200 J laser energy, the transition of the flow field is basically the same as the case of laser-focusing on the cowl. The thrust becomes larger than the one of the case of laser-focusing on the cowl with the same energy. The reason for this is that a stronger shock wave is induced at the point closer to the afterbody, as shown in Fig.8.

With 400 J laser energy, the shock wave is spat out from the inlet, as shown in Fig.9, because the strong shock wave can propagate upstream without disturbance by the cowl. This shock wave acts as drag by sweeping the forebody.

In the case of laser-focusing on the cowl, this shock spit-out does not occur although the laser energy is 600 J. Therefore, in order to prevent the shock spit-out of an actual process involving LSD, the cowl shape needs to be optimized. For example, the inclination of cowl to the inflow should be steeper than the one used in the present computation.

Thrust and Coupling coefficient

Figure 10 shows the axial thrust histories of the case of laser-focusing on the cowl by 200 , 400 and 600 J. After laser-focusing, during initial several micro seconds, the net thrust is negative due to the aerodynamic drag in all cases. Since the inner cowl surface near the focus is parallel to the z axis, the initially strong shock wave, generated on the focus, does not act as thrust. When the shock wave strikes the afterbody, the thrust rapidly increases. The Larger the laser energy, the higher the thrust jump and the earlier it occurs. The thrust has a maximum value while the shock wave leg sweeps the afterbody. After this time, the thrust gradually returns to the value of the drag. The duration, while a positive thrust is maintained, increases with the the laser energy.

Figure 11 shows the case of laser-focusing at the middle point of the flow channel and the case of laser-focusing on the cowl with 200 J energy. The duration, in the case of laser-focusing at the middle point of the flow channel, is about twice as long as the one of laser-focusing on the cowl, because the shock wave is induced at a point closer to the afterbody than the one of laser-focusing on the cowl. Accordingly, the thrust is larger and the thrust jump also occurs earlier than those of laser focusing on the cowl. On the case of laser-focusin on the middle point of the flow channel, the second thrust peak appears near 5μs. This peak is be caused by the pressure increase around the afterbody surface behind the body shoulder, as shown in Fig.12. This pressure increase disappears after a few micro sec.

Figure 13 shows the coupling coefficients estimated in the computations by Wang et al.[3], the experiments by Myrabo et al.[1,2] and the present computations. The coupling coefficient is defined as the following,

$$C_m = \frac{\text{The cumulative impulse}}{\text{One pulse laser energy}}. \qquad (8)$$

In the present computation, the cumulative impulse is calculated as the time integral of the force

increment from the aerodynamic drag. The coupling coefficients in the cases of laser-focusing on the cowl are fairly constant at about 150 N · s/MJ, being independent of the laser energy or slightly decreasing with laser energy. This tendency is the same as the computations by Wang et al. and experiments by Myrabo et al.

In the case of laser-focusing at the middle point of the flow channel, the coupling coefficient is about 2.5 times as large as the one in the case of laser-focusing on the cowl. Therefore, the coupling coefficient is found to be sensitive to the focus location.

The computed shock wave is stronger than the actual one because chemical reactions are neglected here. In order to improve the accuracy of the impulse and coupling coeffcient estimation, it is necessary to include the energy loss mechanisms, chemical reaction and thermal radiation.

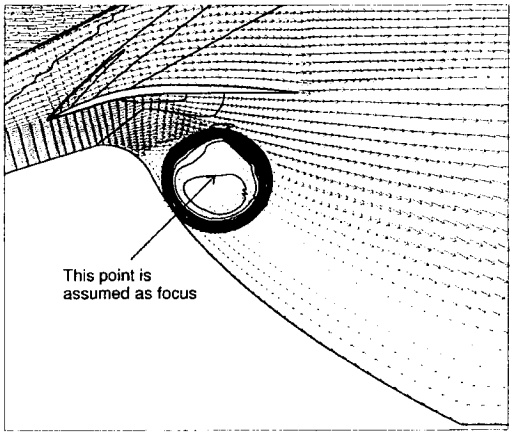

Fig.8 Pressure contours and vector plots at t = 1 μs in the case of laser-focsuing at the middle point of the flow channel with 200 J energy.
(max. = 740595 Pa, min. = 405 Pa, incre. = 14804 Pa)

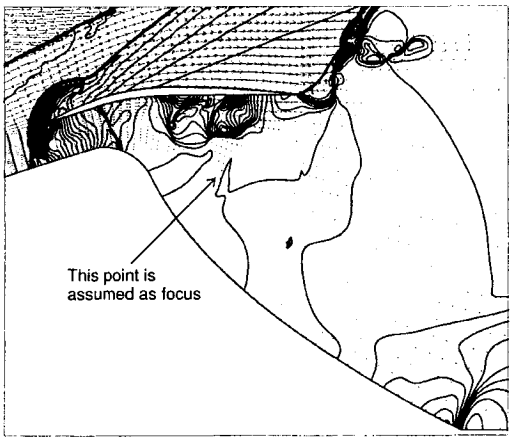

Fig.9 Pressure contours and vector plots at t = 30 μs in the case of laser-focsuing at the middle point of the flow channel with 400 J energy.
(max. = 1207828 Pa, min. = 1399 Pa, incre. = 24129 Pa)

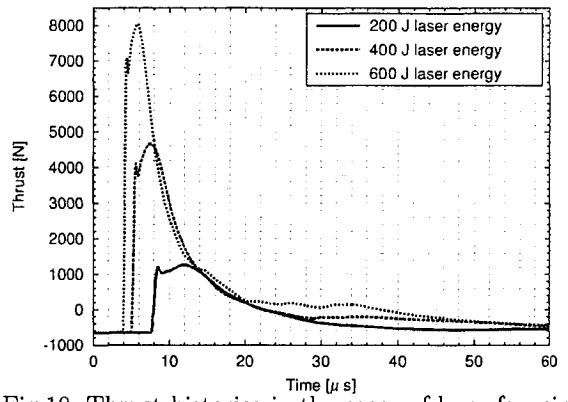

Fig.10 Thrust histories in the cases of laser-focusing on the cowl.

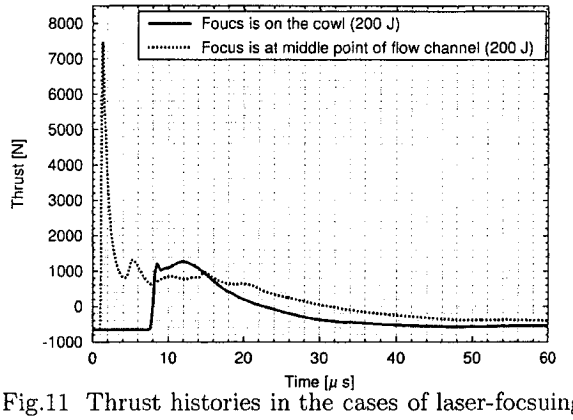

Fig.11 Thrust histories in the cases of laser-focsuing on the cowl and at the middle point of the flow channel with 200 J.

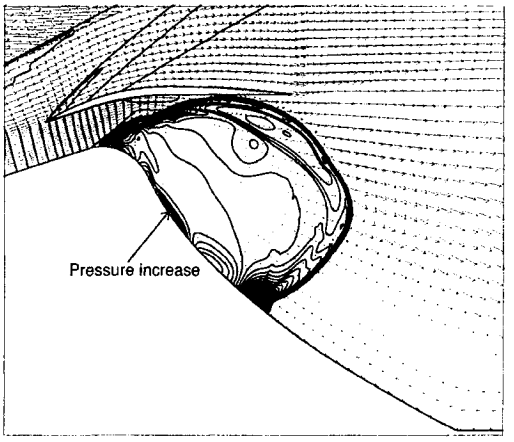

Fig.12 Pressure contours and vector plots at t = 5 μs in the case of laser-focsuing at the middle point of the flow channel with 100 J energy.
(max. = 771276 Pa, min. = 1399 Pa, incre. = 15398 Pa)

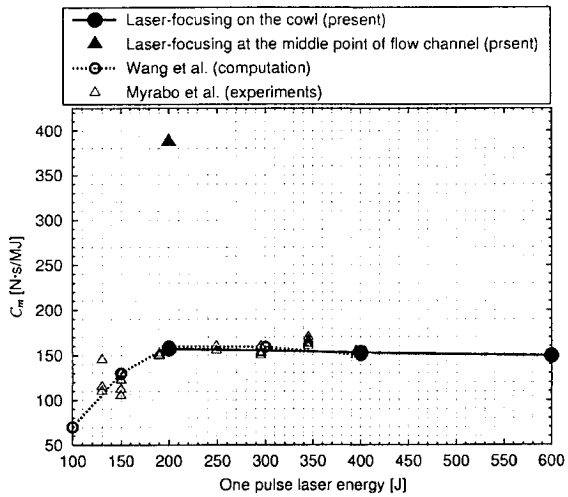

Fig.13 Coupling coefficients.

SUMMARY

The shock wave leg propagating downstream sweeps the afterbody, and provides the main thrust to the body. The shock wave propagating upstream stays near the inlet because the speed of the shock wave relative to the body becomes equal to the inflow speed. This shock wave is finally blown downstream and decays to pressure waves.

The estimated coupling coefficient in the case of laser-focusing on the cowl is fairly constant at about 150N · s/MJ, being independent of the laser energy.

The coupling coefficient is found to be sensitive to the focus location.

REFERENCES

[1] Myrabo, L.N., Messitt, D.G., and Mead, F.B.Jr., "Ground and Flight Tests of a Laser Propelled Vehicle," AIAA Paper 98-1001, Jan., 1998.

[2] Mead, F.B.Jr., Myrabo, L.N., and Messitt, D.G., "Flight and Ground Tests of a Laser-Boosted Vehicle," AIAA Paper 98-3735, 1998.

[3] Wang, T.S., Chen, Y.S., Liu, J., Myrabo, L.N., and Mead, F.B.Jr., "Advanced Performance Modeling of Experimental Laser Lightcrafts," AIAA Paper 2001-0648, Jan., 2001.

[4] Raizer, Y.P., "Breakdown and Heating of Gases under the Influence of a Laser Beam," Soviet Physics USPEKHI, Vol.5, No.8, Mar.-Arp., 1966, pp.650-673.
March-April, 1966.

[5] Raizer, Y.P., "Subsonic Propagation of a Light Spark and Threshold Condition for the Maintenance of Plasma by Radiation," Soviet Physics JETP, Vol.31, No.6, Dec., 1970, pp.1148-1154.

[6] Raizer, Y.P., and Tybulewicz, A., "Laser-Induced Discharge Phenomena," Studies in Soviet Sience, Edited by Vlases, G.C., and Pietrzyk, Z.A., Consultants Bureau, New York, 1977.

[7] Tannehill, J.C., and Anderson D.A., Pletcher, R.H., "Computational Fluid Mechanics and Heat Transfer, 2nd ed.," Tayler & Francis, Levittown, PA, 1997.

[8] Gupta, R.N., Yos, J.M., Thompson, R.A., and Lee, K.P., "A Review of Reaction Rates and Thermodynamic and Transport Properties for an 11-Species Air Model for Chemical and Thermal Nonequilibrium Calculations to 30000 K," NASA RP-1232, 1990.

[9] Wada, Y., and Liou, M.S., "A Flux Splitting Scheme with High-Resolution and Robustness for Discontinuities," NASA TM-106452, 1994.

[10] Anderson, W.K., Thomas J.L., and Leer B.V., "Comparison of Finite Volume Flux Vector Splittings for the Euler Equations," AIAA Journal, Vol.24, No.9, Sep. 1986. pp.1453-1460.

[11] Jameson A., and Yoon, S., "Lower-Upper Implicit Schemes with Multiple Grids for the Euler Equations," AIAA Journal, Vol.25, No.7, July. 1987. pp.929-935.

[12] Fujii, K., "Unified Zonal Method Based on the Fortified Solution Algorithm," Journal of Computational Physics, Vol.118, 1995. pp.92-108.

[13] Messitt,D.G., Myrabo, L.N., Jones, R.A., and Nagamatsu, H.T., "Computational vs. Experimental Performance of an Axisymmetric Hypersonic Inlet for Laser Propulsion," AIAA Paper 91-2547, June, 1991.

[14] Sedov, L.I., "Similarity and Dimensional Methods in Mechanics, 10th ed.," CRC Press, 1993.

[15] Dewey B.M., McMillin, D.J., and Classen, D.F., "Photogrammetry of Spherical Shocks Reflected from Real and Ideal Surfaces," Journal of Fluid Mechanics, Vol.81, Pt.4, 1977. pp.701-717.